environmental microbiology

Environmental Microbiology (2021) **00**(00), 00–00 doi:10.1111/1462-2920.15863

Protistan plankton communities in the Galápagos Archipelago respond to changes in deep water masses resulting from the 2015/16 El Niño

Erika F. Neave,[1,4,5] **Harvey Seim**,[1] **Scott M. Gifford**,[1] **Olivia Torano**,[1] **Zackary I. Johnson**,[2] **Diego Páez-Rosas**[3] **and Adrian Marchetti**[1*]

[1]*Department of Earth, Marine and Environmental Sciences, University of North Carolina at Chapel Hill, Chapel Hill, NC.*

[2]*Marine Laboratory and Biology Department, Duke University, Beaufort, NC.*

[3]*Galápagos Science Center, Universidad San Francisco de Quito, Isla San Cristóbal, Islas Galápagos, Ecuador.*

[4]*Department of Life Sciences, Natural History Museum, London, UK.*

[5]*School of Biological and Environmental Sciences, Liverpool John Moores University, Liverpool, UK.*

Summary

The Galápagos Archipelago lies within the Eastern Equatorial Pacific Ocean at the convergence of major ocean currents that are subject to changes in circulation. The nutrient-rich Equatorial Undercurrent upwells from the west onto the Galápagos platform, stimulating primary production, but this source of deep water weakens during El Niño events. Based on measurements from repeat cruises, the 2015/16 El Niño was associated with declines in phytoplankton biomass at most sites throughout the archipelago and reduced utilization of nitrate, particularly in large-sized phytoplankton in the western region. Protistan assemblages were identified by sequencing the V4 region of the 18S rRNA gene. Dinoflagellates, chlorophytes and diatoms dominated most sites. Shifts in dinoflagellate communities were most apparent between the years; parasitic dinoflagellates, *Syndiniales*, were highly detected during the El Niño (2015) while the dinoflagellate genus, *Gyrodinium*, increased at many sites during the neutral period (2016). Variations in protistan communities were most strongly correlated with changes in sub-thermocline water density. These findings indicate that marine protistan communities in this region are regimented by deep water mass sources and thus could be profoundly affected by altered ocean circulation.

Received 14 July, 2021; revised 28 October, 2021; accepted 1 December, 2021. *For correspondence.E-mail amarchetti@unc.edu; Tel. (+1) 919 843 3473; Fax (+1) 919 962 1254.

Introduction

The Galápagos Archipelago and surrounding waters (1–2 °S, 90–92 °W) are renowned for having diverse, highly productive ecosystems. The need to protect these marine ecosystems led to the establishment of the Galápagos Marine Reserve (GMR) in 1998 (Bensted-Smith, 1998). Despite greater efforts to conserve and study the GMR, the composition of marine protists, which can dominate primary production in this region, remains understudied. Protistan plankton exhibit diverse trophic modes, ranging from autotrophic phytoplankton to heterotrophic flagellates. A shift in protist community composition towards increased heterotrophy can therefore drastically alter the quantity of food available for higher trophic levels, and thus influence the overall productivity of the Galápagos marine ecosystem (Pauly and Christensen, 1995).

The convergence of ocean currents allows waters within the archipelago to have high primary production relative to the surrounding Eastern Equatorial Pacific (EEP) Ocean. In contrast to the archipelago, the EEP is a high-nutrient, low chlorophyll region due to iron limitation (Behrenfeld *et al*., 1996) which is largely relieved in the GMR when currents upwell lithogenic nutrients from the Galápagos platform (Barber and Chavez, 1991; Rafter *et al*., 2017). Three major ocean currents provide the bulk of nutrient sources to the region (Lindley and Barber, 1998; Fiedler and Talley, 2006). The South Equatorial Current is a surface current that flows westward, enveloping the equator, and is fed by the Peruvian coastal upwelling and equatorial upwelling (Pennington *et al*., 2006) (Fig. 1A). The North Equatorial Countercurrent flows eastward at the surface, transporting western Pacific warm pool water to the north of the South

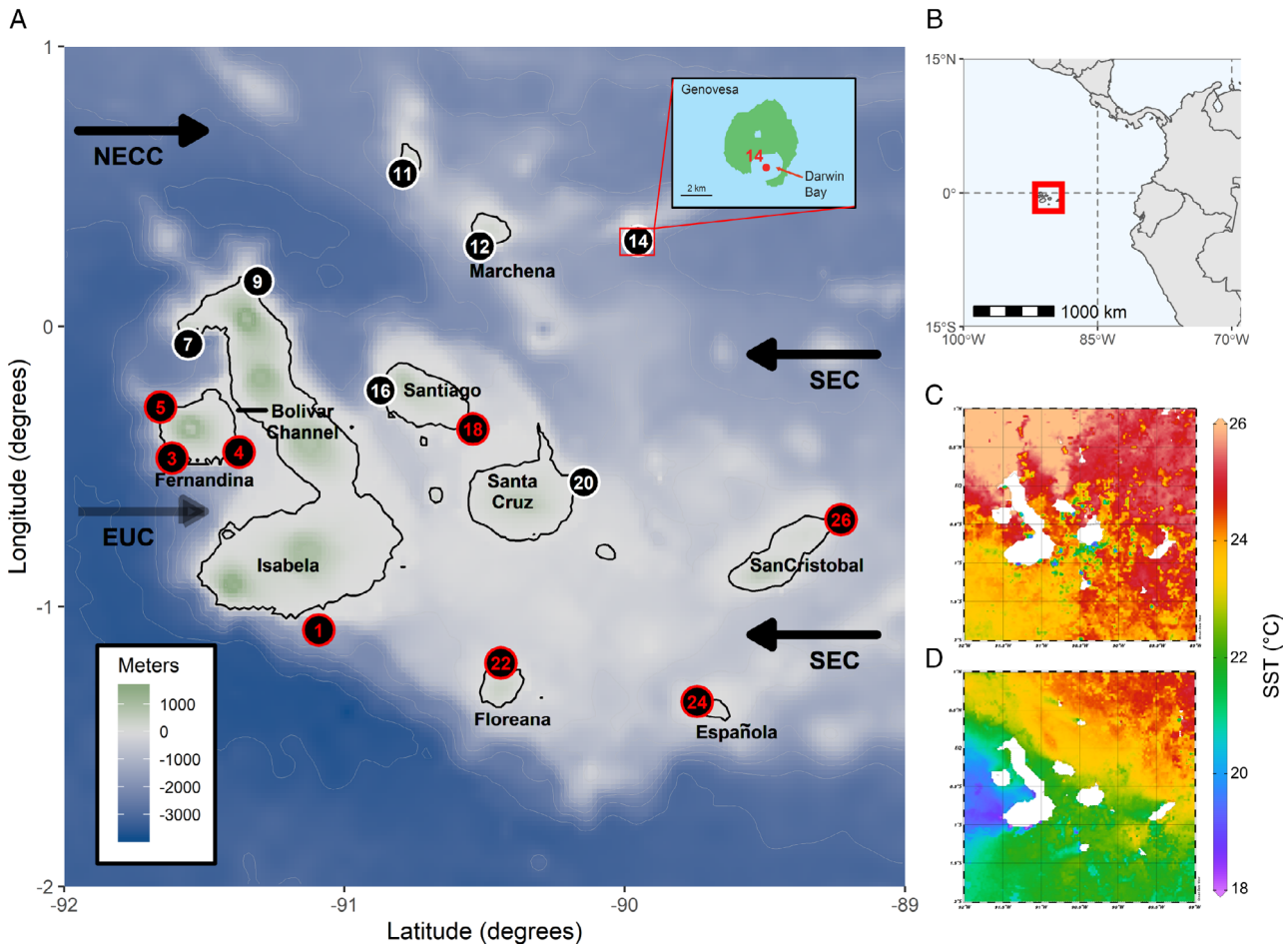

Fig 1. The Galápagos Archipelago study region.
A. Topographic map of the Galápagos Archipelago and sampling locations. White numbers indicate sites which were sampled for oceanographic measurements while red numbers indicate sites that were sampled for oceanographic measurements and protistan community DNA. Currents are abbreviated such that: SEC = South Equatorial Current, NECC = North Equatorial Countercurrent and EUC = Equatorial Undercurrent. Upper right inset shows the location of site 14 near Genovesa Island, a partially collapsed caldera.
B. Map showing the location of the Galápagos Archipelago within the Eastern Equatorial Pacific. Monthly averaged sea-surface temperatures (NOAA AVHRR) throughout the Galápagos Archipelago for the sampling period in (C) October of 2015 and (D) October of 2016. [Color figure can be viewed at wileyonlinelibrary.com]

Equatorial Current. The most critical supply of nutrients to the region comes from the eastward-flowing Equatorial Undercurrent (EUC) that collides subsurface with the western side of the Galápagos platform. It flows around and through the archipelago below the surface layer (Kessler, 2006) carrying nutrient-rich subtropical underwater, and can outcrop west of the archipelago, making this region a primary productivity hotspot (Chavez and Brusca, 1991; Sakamoto *et al*., 1998).

Marine protistan communities in the EEP are influenced by El Niño Southern Oscillation (ENSO), a spatiotemporally complex interannual shift in equatorial Pacific Ocean circulation. The EEP harbours mostly small-sized phytoplankton communities consisting of *Prochlorococcus*, *Synechococcus* and picoeukaryotes (Chavez *et al*., 1996). However, when equatorial upwelling is strong it can provide sufficient iron and silica for large-sized phytoplankton, such as diatoms, to bloom (Pennington *et al*., 2006; Marchetti *et al*., 2010; Masotti *et al*., 2011). During an El Niño event, EEP sea surface temperatures (SSTs) rise above the climatological average causing stratification. This results in weaker equatorial upwelling, a deeper thermocline and a slower EUC. El Niño conditions lead to reduced nitrate availability and decreases in *Synechococcus*, likely because of their high cellular nitrogen requirement (Moore *et al*., 2002), which allow small heterotrophic protists to dominate, altering marine food web dynamics in the EEP (Masotti *et al*., 2011). Contrary to community dynamics in the EEP, on the west side of the Galápagos Archipelago, *Synechococcus* and *Prochlorococcus* concentrations decreased during a neutral period of stronger upwelling

following the 2015/16 El Niño (Gifford *et al*., 2020). Given that *Prochlorococcus* is speculated to prefer nitrogen sources other than nitrate, it may be more competitive under stratified El Niño conditions (Moore *et al*., 2002). There is less understanding of how shifts in photosynthetic eukaryotes and other protists are influenced by ENSO in the Galápagos Archipelago specifically, where increased vertical mixing due to topographic upwelling allows for a relatively higher baseline phytoplankton biomass than the surrounding EEP (Barber *et al*., 1996).

Despite limited knowledge on protistan communities, establishing causes for fluctuations in phytoplankton biomass in the GMR has been investigated previously (Maxwell, 1975; Feldman, 1986). Some studies have used satellite chlorophyll *a* (Chl *a*) proxies to understand phytoplankton biomass variability (Liu *et al*., 2014; Kislik *et al*., 2017). Despite seasonal Chl *a* variability in the GMR, its amplitude varies with basin-scale SST trends, in that Chl *a* peaks in the Boreal spring, synchronous with the strengthening of the EUC (Palacios, 2004; Sweet *et al*., 2007). However, this temporal pattern in Chl *a* amplitude does not hold true spatially, as individual bioregions of the GMR differ (Edgar *et al*., 2004). The South Equatorial Current and the North Equatorial Countercurrent meet forming the equatorial front, the seasonal oscillation of which has been used to predict patterns of Chl *a* concentration (Schaeffer *et al*., 2008). In the latter part of the year, the strengthening and tilt of the equatorial front can largely explain Chl *a* variability (Palacios, 2004).

Fewer studies have focused on observing *in situ* environmental conditions and their influence on protistan community compositional changes (McCulloch, 2011 unpublished; Carnicer *et al*., 2019). These observations are necessary for understanding the ecological implications of El Niño events in this region. Sporadic surveys of phytoplankton communities provide a historical record of common diatoms and dinoflagellate species; however, they are limited to observations of large, more 'charismatic' species easily identified using light microscopy (Torres, 1998; Torres and Tapia, 2000, 2002; Tapia and Naranjo, 2012). Some harmful algal species were identified along with spatial variability in dinoflagellate diversity, which was attributed to changes in deep water masses to the west of the Galápagos platform (Carnicer *et al*., 2019). Accessory phytoplankton pigments have also been used to assess phytoplankton composition in the GMR, such that relative abundances of diatoms and chlorophytes were found to decrease during the 2004/05 El Niño event, while cyanobacteria and haptophyte proportions increased (McCulloch, 2011 unpublished).

In this study, DNA metabarcoding (i.e. sequencing the 18S rRNA [18S] gene) was used to examine protistan community composition during an El Niño (2015) and neutral (2016) years (Fig. 1). Here we show distinct shifts in protist plankton genera in waters of the Galápagos Archipelago and how they correlate with primary productivity and oceanographic variables during the 2015/16 ENSO cycle. Because protistan plankton are important links between oceanographic processes and marine food webs, it is imperative to understand how these factors influence their composition and production, particularly with shifts in environmental conditions attributed to climatic events.

Results and discussion

Physical seawater properties

Differences in upper ocean physical seawater properties between the El Niño (2015) and neutral (2016) years were apparent (Fig. 2, Supporting Table 1). At most sites, mixed layer depths were deeper in 2015 than in 2016 (Fig. 2A). The mixed layer temperature range was warmer in 2015 (22.9–26.4°C) relative to 2016 (17.1–23.7°C), with a mean difference of 3.8°C (Fig. 2B). Mixed layer salinities varied by an average of 0.23 PSU, with most being higher in 2015 (Fig. 2C). As a result, the mean density in 2016 was higher by 0.99 kg m^{-3} during the neutral period (Fig. 2D). These differences in densities also existed spatially, such that the sites located west of Isabela Island (Sites 3–7) had the highest mixed layer density values in 2016 (Fig. 2D). Similar interannual density trends were observed in the subthermocline layer, where subthermocline depths at most sites were deeper in 2015 than in 2016 (Fig. 2E). The subthermocline layer was on average 3.2°C cooler and 0.07 PSU fresher in 2016 resulting in seawater which was on average 0.70 kg m^{-3} denser relative to the El Niño (Fig. 2F–H). One notable exception was site 14 located near Genovesa Island, inside a partially submerged caldera (see inset map in Fig. 1A). The caldera is isolated from the surrounding ocean by an approximately 10 m deep sill, restricting exchange with waters outside the caldera and allowing seawater properties within the caldera to remain more constant between years. Aside from this site outlier, subthermocline layer densities showed consistent temporal change relative to the mixed layer, which was more spatially sensitive.

The differences in water mass densities between the years were reflected in dissolved nutrient concentrations. Nitrate and silicic acid ($Si[OH]_4$) concentrations within the mixed layer were lower at nearly all sites in 2015 relative to 2016 (Fig. 3A and B). Nitrate concentrations in the euphotic zone were significantly lower during the El Niño relative to 2016, with median values of 1.70 and 6.20 μmol L^{-1} respectively (Fig. 3C). Similarly, $Si(OH)_4$

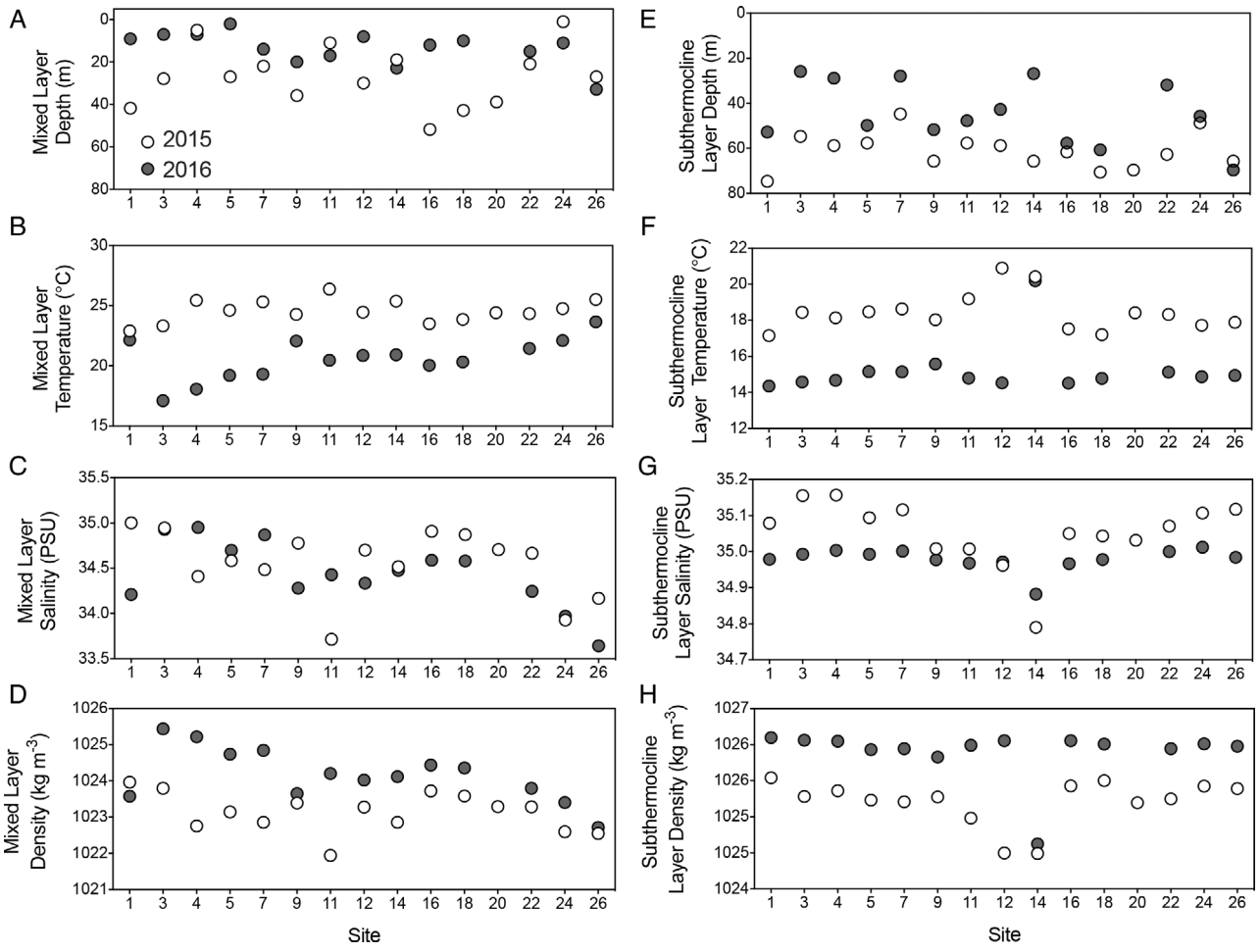

Fig 2. Physical seawater properties during the 2015 and 2016 sampling periods.
A. Mixed layer depths, (B) mixed layer temperatures, (C) mixed layer salinities, (D) mixed layer densities, (E) subthermocline layer depths, (F) subthermocline layer temperatures, (G) subthermocline layer salinities and (H) subthermocline layer densities.

had lower median values in 2015 (1.65 μmol L^{-1}) compared to 2016 (4.99 μmol L^{-1}) (Fig. 3D). Both years had higher NO_3^- concentrations relative to $Si(OH)_4$ concentrations; however, the slope of the $Si(OH)_4$: NO_3^- distribution in 2015 was lower ($m = 0.40$) than in 2016 ($m = 0.69$), indicating that the concentration of $Si(OH)_4$ relative to NO_3^- was lower during the El Niño (Fig. 3E). Overall, physical seawater properties and nutrient concentrations in the GMR show strong temporal trends indicative of oceanographic variation during the 2015/16 El Niño event.

Phytoplankton biomass and primary productivity

Chl *a* concentrations were higher in 2016 at most sites with the exceptions of sites 14 and 16 (Fig. 4A). The median concentration of the small-size fraction (<5 μm) was similar between 2015 (0.22 μg L^{-1}) and 2016 (0.23 μg L^{-1}) (Fig. 4B). The large-size fraction (>5 μm) had a higher median in 2016 (0.2 μg L^{-1}) relative to 2015 (0.13 μg L^{-1}) with a maximum concentration of 1.43 μg L^{-1} in 2016 (Fig. 4C). These are comparable to measurements (89–92 °W, 2 °S–1°N) observed previously during a neutral period, where the average surface Chl *a* was 0.25 μg L^{-1} and the highest concentration (0.53 μg L^{-1}) was recorded west of Isabela island (Torres and Tapia, 2000). In our study, the average small and large size fractions of Chl *a* did not significantly differ between years; however, the large size fraction showed stronger temporal ($p = 0.06$) and spatial trends, having higher concentrations in 2016 at sites located west of Isabela Island (Fig 4A and D).

Synechococcus flow cytometry cell counts were higher at western sites 3–7 in 2015 than in 2016 (Supporting Fig. 1), similar to observations made at the same sites quantified using metagenomics (Gifford *et al*., 2020). Site 4 had the greatest difference between the years, having a concentration of 2.4 $\times 10^5$ cells ml^{-1} in 2015 and

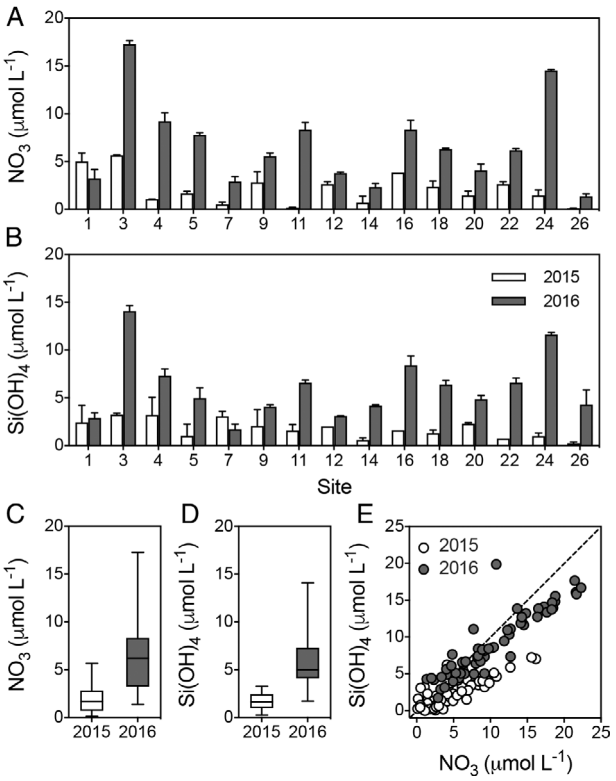

Fig 3. Dissolved inorganic nutrients during the 2015 and 2016 sampling periods.
A. Nitrate (NO_3^-) concentrations.
B. Silicic acid ($Si[OH]_4$) concentrations.
C. Interquartile range of NO_3 concentrations at the 50% incident irradiance depth.
D. Interquartile range of $Si(OH)_4$ concentrations at the 50% incident irradiance depth.
E. Scatter plot of NO_3^- versus $Si(OH)_4$ concentrations collected at depths (50%, 30%, 10%, 1% incident irradiance depths) throughout the euphotic zone. The dashed line represents the 1:1 line. Error bars indicate the standard deviation of the mean ($n = 2$).

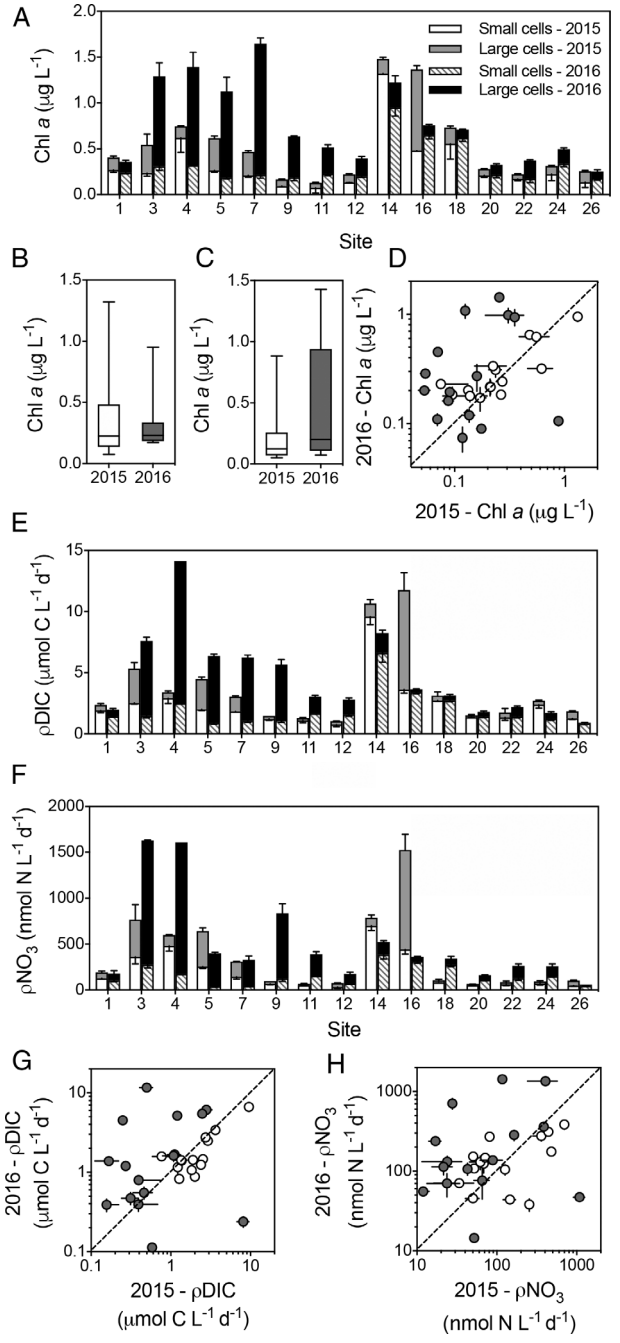

Fig 4. Phytoplankton biomass and primary productivity at the 50% incident irradiance depth during the 2015 and 2016 sampling periods. A. Size-fractionated chlorophyll *a* (Chl *a*) concentrations. Chl *a* is distinguished between large (>5 μm) and small (<5 μm) size fractions. B. Interquartile range of Chl *a* concentrations in small cells across all sites and (C) interquartile range of Chl *a* concentrations in large cells across all sites. D. Scatter plot of large (grey) and small (white) cell Chl *a* concentrations in 2016 versus 2015. Size-fractionated (E) dissolved inorganic carbon uptake rates (i.e. primary productivity; ρDIC) and (F) NO_3^- uptake rates (ρNO_3^-). Bar colours are the same as in A. Scatter plot of size-fractionated (G) ρDIC and (H) ρNO_3^- in 2016 versus 2015. The dashed lines represent the 1:1 line. Symbol colours are the same as in D. Error bars indicate the standard deviation of the mean ($n = 3$). In A, E and F, error bars for the small size fraction are in the downward direction, whereas error bars for the large size fraction are in the upward direction.

5.9 $\times 10^4$ cells ml^{-1} in 2016. The highest *Synechococcus* concentration (2.6 $\times 10^5$ cells ml^{-1}) was recorded in 2015 at site 14, within the isolated caldera. *Prochlorococcus* was generally more abundant in 2015, particularly in the central and eastern sites, and ranged in concentration from 6.2 $\times 10^3$ to 1.9 $\times 10^5$ cells ml^{-1} (Supporting Fig. 1). In 2016 *Prochlorococcus* concentrations were generally lower, ranging from 3.8 $\times 10^3$ to 1.6 $\times 10^4$ cells ml^{-1} except at sites 5 and 7 where they were an order of magnitude lower. Picoeukaryotes typically ranged from 10^3 to 10^4 cells ml^{-1} and had more complex abundance patterns between years than *Synechococcus* and *Prochlorococcus* (Supporting Fig. 1). For example, there were higher concentrations of picoeukaryotes at western sites 4–7 in 2015, while lower concentrations relative to 2016 were recorded at sites 20–26.

Total dissolved inorganic carbon (DIC) uptake rates (primary productivity) remained commensurate between

years but showed spatial variability, such that sites 3–12 and 18–22 increased during 2016 while other sites decreased (Fig. 4E). Insignificant temporal trends in total primary productivity could be attributed to opposite trends in the phytoplankton size fractions. For instance, median DIC uptake rates in the large size fraction were 0.46 μmol C L d^{-1} in 2015 compared to 1.2 μmol C L d^{-1} in 2016, while the small cells decreased from having a median of 1.9 μmol C L d^{-1} in 2015 to 1.44 μmol C L d^{-1} in 2016 (Fig. 4G). NO_3^- uptake rates displayed trends similar to Chl *a* and primary productivity such that the large size fraction differed more between years than the small size fraction ($p = 0.07$; $p = 0.87$) (Fig. 4F and H). The decrease in biomass of the large size fraction in 2015 coincided with a lower median NO_3^- uptake rate (51.9 nmol N L d^{-1}) in the large size fraction compared to the small size fraction (81.4 nmol N L d^{-1}) (Fig. 4H). Overall median rates of NO_3^- uptake were greater in both size fractions during 2016 (129.8, 131.6 nmol N L d^{-1}; small and large size fractions respectively) (Fig. 4H).

Shifts in protistan community composition

The most proportionally dominant protist groups in the GMR included the dinoflagellates (part of the Alveolata group), chlorophytes, diatoms (part of the Stramenopiles group), Hacrobia, Opisthokont fungi and Rhizaria (Fig. 5A). Collectively, dinoflagellates, chlorophytes and diatoms dominated the protistan communities and exhibited the most variability between years (Fig. 5B–D). Other groups had high spatial variability across sites. For instance, the ciliates and rhizarians were detected at every site in 2015 but lacked detection or genus level identification at over half of the sites in 2016 (Supporting Fig. 2a and b). Thus, analyses were focused on changes in the dinoflagellates, chlorophytes and diatoms.

The dinoflagellates had a total of 186 OTUs within 21 genera. Dinoflagellate communities were most represented by seven primary order and genus level groups (Fig. 5B). Temporal changes in dinoflagellate proportions between years were more prominent than spatial changes among sites, as indicated by a larger variation along the horizontal axis of the NMDS plot (Fig. 6). Changes in dinoflagellate community structure most resembled the collective changes in the density of the subthermocline layer, primary productivity by small cells and picoeukaryote cell abundance (Spearman's $\rho = 0.61$) (Table 1). Dinoflagellate composition changed the most between years relative to the chlorophytes and diatoms, yet as a broader group they maintained relatively high proportions over the 2015/16 ENSO. This could be due in part to the diverse life strategies that enable dinoflagellates to bloom at various phases of the upwelling cycle (Smayda and Trainer, 2010). Another consideration is the interspecific variability in rRNA gene copy number among the different protist groups. Dinoflagellates, for example, tend to have higher 18S rRNA gene copy numbers than other eukaryotic groups, but there is not enough empirical data to speculate on the implications of this beyond our observations (Lavrinienko *et al*., 2021).

Members of the dinoflagellate genus *Gyrodinium* showed the strongest temporal shift, seeming to favour the relatively cooler, higher nutrient conditions present in 2016 such that they were notably represented in the west (sites 3–5) and east (sites 22–26) (Fig. 5B). Some *Gyrodinium* species, most of which being heterotrophic, have been found in sediments, and are suspected to form benthic resting cysts which live on internal nutrient reserves for long periods of dormancy until conditions become more favourable for growth, i.e. ample prey availability (Shang *et al*., 2019). Along the coasts of Santa Cruz and other small neighbouring islands in the central region of the GMR, water column surveys of dinoflagellate communities found that 84% of samples contained benthic epiphytic dinoflagellates (Carnicer *et al*., 2019), a high percentage given that only ~10% of dinoflagellates associate with a substrate (Hoppenrath *et al*., 2014). The suspension of these dinoflagellates in the GMR suggests potential physical mechanisms for benthic resting cyst resuspension. Other cyst forming genera that were detected in our samples included *Alexandrium*, *Gonyaulax*, *Neoceratium*, *Paragymnodinium*, *Peridinium*, *Protoperidinium* and *Woloszynskia* (Pospelova and Head, 2002; Bravo and Figueroa, 2014; Yokouchi *et al*., 2018). *Peridinium* was also detected in 2016 at sites 22 and 24, where it made up a significant proportion of the dinoflagellate community (Fig. 5B). Long-term nutrient and temperature stress are the most common causes of resting cyst formation in dinoflagellates (Bravo and Figueroa, 2014). For example, *Gyrodinium uncatenum*, now renamed *Levanderina fissa*, forms cysts to survive in a dormant resting stage which can last for a duration of months to decades (Anderson *et al*., 1985). This and other direct observations of cyst formation in closely related species suggest that the *Gyrodinium* genus have the ability to survive long-term environmental stress (Bravo and Figueroa, 2014; Shang *et al*., 2019). Therefore, resting cyst formation may be an important strategy for dinoflagellates to subsist over El Niño events.

Syndiniales are a group of parasitoid dinoflagellates that survive via dinoflagellate or metazoan hosts (Jephcott *et al*., 2016). Metabarcoding techniques have revealed that these parasites are more prevalent than previously recognized (Guillou *et al*., 2008), and this too is the case in the GMR. Syndiniales groups I and II were

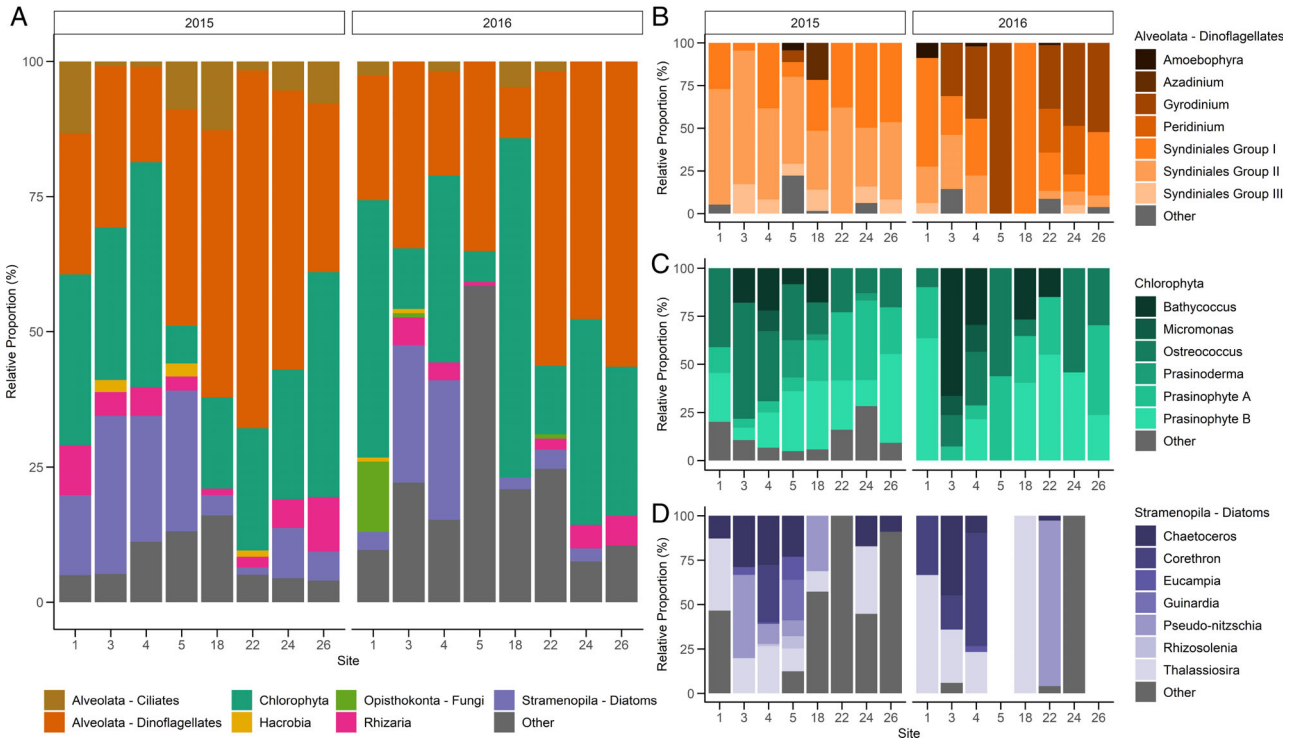

Fig 5. Protistan community composition based on 18S rRNA gene amplicons.
A. Relative proportions of protists at class level groupings in 2015 and 2016. Relative proportions of the (B) Dinoflagellate group, (C) Chlorophyta group and (D) Diatom group highlighting the top seven most abundant genera in each group. [Color figure can be viewed at wileyonlinelibrary.com]

dominant in 2015; both groups were simultaneously detected in 2016 except at sites 5 and 18. In 2016, site 18 notably had a dinoflagellate community highly dominated by Syndiniales I. Syndiniales III covered a larger spatial extent in 2015 than 2016 but generally followed the same trend as Syndiniales I and II, such that relative proportions were typically less in 2016 (Fig. 5B). One caveat of our metabarcoding approach is that it does not distinguish between free-living cells and host-associated parasites, which makes the ecological role of Syndiniales difficult to assess. Notwithstanding, higher relative proportions of Syndiniales during the El Niño may be a result of increased infection rates since host cell death precedes the release of Syndiniales spores (Jephcott *et al*., 2016; Clarke *et al*., 2019). *Ameobophyra*, a specific Syndiniales genus identified in the GMR (Fig. 5B), is estimated to use half of its host's biomass for spores leaving the other half as particulate and dissolved organic matter (Salomon and Stolte, 2010; Jephcott *et al*., 2016). Consistent with some Syndiniales exploiting photosynthetic hosts, Syndiniales I has been found to correlate positively with Chl *a*, perhaps implying its association with high host biomass or productive regions (Clarke *et al*., 2019). Despite the high detection of Syndiniales, particularly during the El Niño, their effect on primary productivity and food web dynamics remains unclear.

The Chlorophyta or green algae had a total of 163 identified OTUs within six genera. The six genera are displayed with an 'other' group, which consists of chlorophytes that could not be identified to the genus level (Fig. 5C). The most common genera was *Bathycoccus*, the subclades A and B from clade VII of the prasinophytes (Lopes Dos Santos *et al*., 2017), which we refer to as Prasinophyte A and Prasinophyte B, and *Ostreococcus*. Prasinophyte A and B made up a large relative proportion at many of the sites (Fig. 5C), consistent with other studies within the EEP region (Collado-Fabbri *et al*., 2011; de Vargas *et al*., 2015).

Spatial variation in chlorophyte communities was more apparent than shifts associated between years. Prasinophyte A, Prasinophyte B and *Ostreococcus* were detected at all sites in 2015. Similarly in 2016, these groups were detected at most sites apart from sites 5, 22 and 24 which respectively lacked detection of either Prasinophyte B, *Ostreococcus*, or Prasinophyte A. Regardless of year, proportions of prasinophytes were generally highest in the east and slightly decreased westward (Fig. 5C). *Ostreococcus* are cosmopolitan in

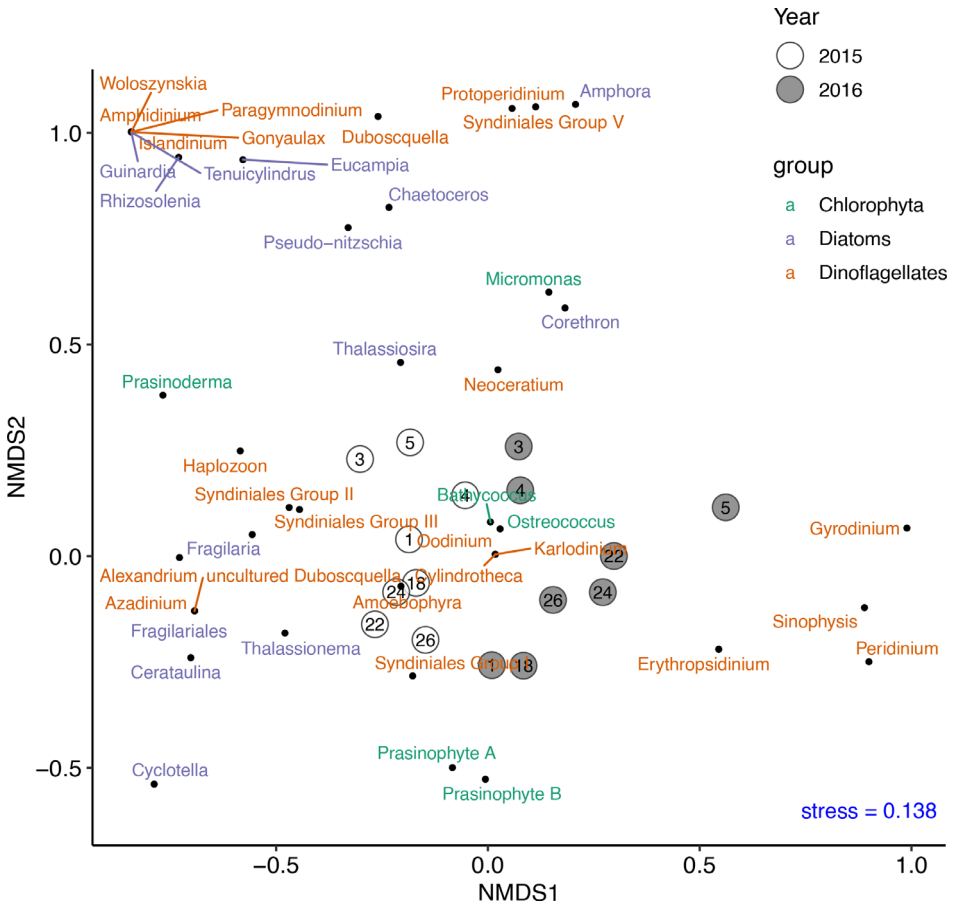

Fig 6. Non-metric multi-dimensional scaling (NMDS) plot showing differences in the whole protistan community composition based on the Bray–Curtis dissimilarity matrix. 2015 sites (white) and 2016 sites (grey) are labelled with site numbers. The loadings for each genera group are plotted as points (black). [Color figure can be viewed at wileyonlinelibrary.com]

Table 1. Combinations of variables yielding the 'best matches' of variable (Euclidian) and community (Bray–Curtis dissimilarity) matrices using Spearman's rank correlation (ρ).

Community	Environmental and ecological variables	Variables	Spearman's ρ
Whole	Total NO_3^- uptake, PicoEuk, Pro, density of subthermocline	4	0.6239
Whole	Syn, density of subthermocline	2	0.5664
Whole	Density of subthermocline	1	0.3681
Dinoflagellates	Small DIC uptake, PicoEuk, density of subthermocline	3	0.6063
Chlorophytes	Total NO_3^- uptake, PicoEuk	2	0.6826
Diatoms	Small DIC uptake, Pro	2	0.3671

The variables are abbreviated such that: Total NO_3^- uptake = total nitrate uptake of both large and small phytoplankton size fractions; PicoEuk = picoeukaryote flow cytometry counts; Pro = *Prochlorococcus* flow cytometry counts; pden_dl = potential density of the subthermocline layer; Syn = *Synechococcus* flow-cytometry counts; Small DIC uptake = dissolved inorganic carbon uptake by the small (<5 μm) phytoplankton size fraction. Abbreviated; for full version, see Supporting Table 6.

protistan communities of the Peruvian coastal upwelling, and thus thrive under upwelling conditions, which could explain a higher detection at sites associated with the EUC (Collado-Fabbri *et al*., 2011; Rii *et al*., 2016). Moreover, total NO_3^- uptake rates and picoeukaryote cell abundance (via flow cytometry) best explained changes in chlorophyte communities (Spearman's $\rho = 0.6826$) (Table 1); the latter being expected given that many chlorophytes are small enough to be enumerated as picoeukaryotes. Chlorophyte communities showed the most spatial changes relative to the dinoflagellates and diatoms, such that genera spread along the vertical axis of the NMDS plot (Fig. 6).

The diatoms consisted of 78 identified OTUs within 15 genera. Diatom communities were well represented with seven genera and an 'other' group that mainly were comprised of those unidentifiable to the genus level (Fig. 5D). Diatoms were not detected through 18S rRNA

gene sequencing at sites 5 or 26 in 2016 but may have been present at low abundances. Patterns of primary productivity by small cells and *Prochlorococcus* cell abundance provided the best prediction of diatom community change (Spearman's $\rho = 0.3671$) (Table 1). Given the patchy spatial extent of diatoms detected, the ability to predict the changes in the diatom community from the oceanographic variables was lower relative to the other examined plankton groups.

Two common diatom genera, *Corethron* and *Pseudo-nitzschia*, had slight temporal trends and are hypothesized to be somewhat regulated by the EUC upwelling conditions (Torres and Tapia, 2000; McCulloch, 2011 unpublished). During 2015, *Pseudo-nitzschia* was present at the western sites (sites 3–5) and site 18. Similarly, during the 2006/07 El Niño, *Pseudo-nitzschia* was a dominant phytoplankton species north and west of Isabela Island (McCulloch, 2011 unpublished). *Pseudo-nitzschia* was, however, still highly detected in 2016 at site 22. In prior neutral periods, this diatom genus has been observed in patchy distributions (Torres and Tapia, 2000; Tapia and Naranjo, 2012). *Corethron* followed opposite trends, such that it represented a higher proportion at sites 1, 3 and 4 in the neutral period while in 2015 it was only detected at site 4. Similarly, a 10-fold decrease in *Corethron* was measured during the 2006/07 El Niño relative to its highest abundance during cooler, neutral periods (McCulloch, 2011 unpublished). *Pseudo-nitzschia* species are detected in the diatom community even in low nutrient conditions, likely due to physiological advantages, while *Corethron* are present in greater proportions at sites 1–4 in 2016, likely benefitting from the nutrient-rich neutral period. Two other ubiquitous diatom genera, *Chaetoceros* and *Thalassiosira*, were omnipresent in the GMR and have been previously identified during various seasons and stages of ENSO (Torres and Tapia, 1998; McCulloch, 2011 unpublished; Tapia and Naranjo, 2012; Naranjo and Tapia, 2015). *Chaetoceros* can form resting spores anticipatory of relaxation periods (Pitcher *et al*., 1991), fair well under horizontal advection (Tilstone *et al*., 2015), and germinate rapidly (Smayda, 2000), which may explain their higher proportions at western sites in both 2015 and 2016 (Fig. 5D).

Deep water mass properties influence protist communities

The protistan community varied most between the El Niño and neutral periods but also had some spatial patterns, such that western and eastern sites formed groupings (Fig. 6). From the BIO-ENV analysis, this variation in protistan community composition is best explained (Spearman's $\rho = 0.6239$) collectively by patterns of total NO_3^- uptake, picoeukaryote and *Prochlorococcus* cell abundances, and the density of subthermocline layer water masses (Table 1). Interestingly, *Synechococcus* abundance and density of the subthermocline layer had the highest BIO-ENV model predictability of any two variables combined ($\rho = 0.5664$) (Table 1). Moreover, regressions between select individual variables and community dissimilarities showed that *Synechococcus* had the highest correlation with community change ($R^2 = 0.7271$), due to its significant correlation with dinoflagellate and chlorophyte community subgroups (Supporting Table 2). Dinoflagellates, the subgroup of the protistan community which varied the most, also had the strongest correlation with the density of the subthermocline layer ($R^2 = 0.73$) (Supporting Table 2).

In the broader EEP, phytoplankton biomass has been linked to changes in deep water mass conditions below the thermocline, such that decreases in Chl *a* biomass due to El Niño events can be detected before SST anomalies (Park *et al*., 2018). Thermocline depth has also previously been identified as important for predicting Chl *a* concentrations in the GMR (Palacios, 2002; Sweet *et al*., 2007). In this study, the lack of strong correlation between the protistan communities with mixed layer properties is likely due to protists, particularly dinoflagellates, responding to deep water mass shifts before they are detected in the mixed layer. The EUC, a deep nutrient-rich current that slows during El Niño, not only upwells on the western side of the Galápagos platform but flows horizontally around Isabela Island and continues eastward, providing deep water mass sources from the north and south to the archipelago (Jakoboski *et al*., 2020). The EUC likely influenced the observed spatiotemporal changes in protistan communities over the 2015/16 El Niño. These observations also provide support that protistan communities change in conjunction with cyanobacteria populations, and that the density of the subthermocline layer is a critical environmental indicator of that shift in community composition, both of which are attributes of the broader EEP (Masotti *et al*., 2011; Park *et al*., 2018).

Conclusions

Changes in water density profiles coupled with the nutrient regime suggest an observed weakening of the EUC, selecting for different phytoplankton size classes over the 2015/16 ENSO. In 2015, waters were less dense and had lower $Si(OH)_4$:NO_3^- ratios relative to the cooler, 2016 neutral period. Increased nutrient availability in 2016 likely led to increases in nitrate utilization by large cells such as diatoms and dinoflagellates. Despite appreciably lower primary productivity at western sites in 2015

compared to 2016, overall primary productivity did not significantly differ across the entire archipelago due to local hotspots during El Niño (e.g. sites 14, 16) and small phytoplankton having higher primary productivity in 2015 at many stations.

Protistan communities varied distinctly in the GMR during the 2015/16 ENSO. Chlorophytes were detected in high abundance in both years, varied spatially, and correlated with NO_3^- uptake, picoeukaryote abundance, and *Synechococcus*. Diatoms had a patchy spatial extent making causes for changes difficult to discern, yet primary productivity by small cells and *Prochlorococcus* abundances were significant correlates. The largest difference between protistan communities, however, was in the dinoflagellate group, such that Syndiniales were highly detected in 2015 while *Gyrodinium* was dominant in 2016. Dinoflagellates also happened to correlate strongly with primary productivity of small phytoplankton, picoeukaryote abundance and the density of the subthermocline layer.

The strongest correlation between the oceanographic variables and the entire protistan community composition over the 2015/16 ENSO was the density of the subthermocline layer – a proxy for shifts in deep water masses. These findings indicate that the water mass sources are an important factor in influencing protistan seed populations in the mixed layer, whereas fluctuations in the short-term oceanographic conditions may have a more profound influence on their overall abundance and physiological status. Our observations provide motivation to continue to elucidate the effects of El Niño events on the microbial food webs in the Galápagos Archipelago and the surrounding EEP region; specifically, to identify how changes in productivity and protistan community composition, as a function of altered ocean circulation, will influence higher marine trophic levels.

Experimental procedures

Sample collection

Fifteen sites within the GMR (89–92 °W, 1.5 °S–2 °N) were sampled over October 10th to 24th of 2015 and October 19th to November 11th of 2016 (Fig. 1A and B). Based on the Oceanic Niño Index and the location of the GMR, situated within both the Niño 1.2 region (80–90 °W, 0–10 °S) and the Niño 3 region (150–90 °W, 5 °N–5 °S), our sampling periods occurred during El Niño (2015) and neutral conditions (2016) (Santoso *et al*., 2017). Remote sensing of SSTs in the region indicates significantly warmer surface waters during the sampling period in 2015 relative to 2016 (Fig. 1C and D). Using a Seabird SBE 19plus V2 SeaCAT Profiler, CTD profiles of temperature, salinity and photosynthetically active radiation (PAR) were collected to ~100 m depth. At each station, following the CTD cast, two separate casts of two 10-L Niskin bottles set up in series were used to collect seawater from the euphotic zone at 50%, 30%, 10% and 1% incident irradiance (I_o) depths, as determined from the station PAR profile, to measure dissolved inorganic nutrients, Chl *a*, DIC and nitrate (NO_3^-) uptake rates, and picoplankton cell counts. Seawater was dispensed into acid-cleaned, seawater-rinsed 10 L Cubitainers (Hedwin Corporation, Newark, DE, USA) and subsampled for measurements. Additional seawater was collected from 50% I_o to obtain DNA (Fig. 1A). Not all sites yielded DNA concentrations sufficient for sequencing. Processed filters and samples were frozen at −20°C until onshore analysis.

Seawater properties

Temperature, salinity and density values were binned per meter from CTD cast measurements. Temperature and salinity profiles were used to determine the depths of the mixed and subthermocline layers. All CTD casts were corrected using SeaBird's SeaSoft software. Potential density (referred to as 'density' in the results and discussion) was calculated using the sw_pden() function from the Mixing Oceanographic toolbox v 1.8.0.0 in MATLAB (R2017b). A consistent density structure was observed, of a surface and deep layer of almost uniform density, separated by a density gradient (interfacial layer) that was typically 10s of meters thick. The surface mixed layer depth was defined as the depth at which the change in density from the surface was >0.35 kg m^{-3}. The subthermocline layer depth (the top of the deep layer of uniform density) was determined by calculating the depth at which change in density from the bottom of the cast was >0.2 kg m^{-3}. The casts were visually inspected to ensure that the density cut-off values defined the layers appropriately. Remote sensing data were obtained from the NOAA CoastWatch Browser and plotted using Ocean Data View. Plots are monthly averaged sea-surface temperatures (NOAA AVHRR) during the cruise periods. Methods for measuring dissolved inorganic nutrients are described in the supporting material.

Phytoplankton biomass and productivity

Phytoplankton biomass was approximated by measuring size-fractioned (<5 and >5 μm) Chl *a* concentrations using the acetone extraction method (Sartory and Grobbelaar, 1984). Picophytoplankton cells, specifically *Prochlorococcus*, *Synechococcus*, and picoeukaryote populations were enumerated using flow cytometry (Johnson *et al*., 2010). Size-fractionated DIC (i.e. primary productivity) and NO_3^- uptake rates were measured from

24 h incubations using stable isotope tracer techniques (Dugdale and Goering, 1967; Hama *et al*., 1983). Since larger-sized phytoplankton groups such as diatoms and dinoflagellates are generally >5 μm, a 5 μm pore size was used to differentiate biomass and uptake rates between these larger phytoplankton taxa and smaller taxa such as cyanobacteria, chlorophytes and other small flagellates. Additional methods describing Chl *a*, flow cytometry, primary productivity and NO_3^- uptake measurements are provided in the supporting material.

DNA sequencing and bioinformatics

Protistan taxonomic identification and proportions were obtained through sequencing the V4 region of the 18S rRNA gene. DNA collection and amplicon library preparation are described in the supporting material. Approximately four million paired-end reads were obtained using the Illumina MiSeq sequencing platform across two lanes. Mean amplicon length for sequencing lane one was 561 bp, while mean amplicon length for sequencing lane two was 599 bp. Sequence files were demultiplexed. QIIME 2 v.2018.6 software was used for processing the raw reads into assembled amplicons. The QIIME 2 plug-in, DADA2 was used for denoising such that reverse and forward reads were truncated to 250 base pairs (bp) and 210 bp, and 260 bp and 280 bp, for sequencing lanes one and two respectively. Chimaeras were removed by the consensus method and reads were merged (Supporting Table 3) using default scripts provided in the QIIME 2 documentation (docs.qiime2.org). Assembled amplicons were annotated by a BLAST search against the SILVA v. 123 reference database using a 90% pairwise identity cutoff. Metazoans were removed. Using the R package phyloseq v. 1.24.2, the samples were rarefied to 2066 reads per site (Supporting Fig. 3).

Annotations which were unknown in the highest taxonomic ranks (Kingdom, Phylum, Class, Order) were removed, under the assumption that it was unlikely to sample a novel high taxonomic rank of plankton. Custom taxonomy was assigned to the Class taxonomic rank based on the top seven relatively abundant groupings (Supporting Table 4). Any annotation that did not belong to the top seven groups was annotated as 'Other'. Unknown or uncultured annotations in the lowest three taxonomic ranks (Family, Genus, Species) were grouped into the 'Other' category within their respective Class ranks. Additionally, where possible, the top seven genera were maintained while the rest were also annotated as 'Other' (there were only six known genera in the Chlorophyta). This resulted in 120 genera, prior to grouping unknown and uncultured OTUs (Supporting Table 3). All raw sequences have been deposited in the NCBI SRA database (Accession No. PRJNA689599).

Statistical analyses

Analysis of water properties, phytoplankton biomass, productivity and 18S rRNA gene data was performed using the vegan package (v. 2.5–4) in R version 3.6.2. Summary statistics and Mann–Whitney–Wilcoxon tests were used to test for differences in dissolved nutrients, Chl *a*, primary productivity and NO_3^- uptake rates between the two sampling years (Supporting Tables 5–11). The 18S rRNA gene data were arranged in an OTU table and transformed to relative proportions at the genus level, from which Bray–Curtis dissimilarity distances were calculated using the vegdist() function. All other variables (i.e. physical water properties, phytoplankton biomass, primary productivity and NO_3^- uptake rates) were similarly transformed to Euclidean distances. A correlation matrix was used to assess which variables were redundant (Supporting Fig. 4). Redundant variables were removed from the BIO-ENV ('biota-environment') analysis. For example, nitrogen and phosphate were correlated with silicic acid (Spearman's $\rho = 0.8$), while temperature of the subthermocline layer was negatively correlated with the density of the subthermocline layer. Therefore, silicic acid and the density of the subthermocline layer were kept in the BIO-ENV analysis, whereas the other variables were removed. The bioenv() function was used to find the best subset of variables which had the maximum rank correlation with the community Bray–Curtis dissimilarities (Clarke and Ainsworth, 1993). These variable subsets were identified for the entire protistan community and for the following subgroups of the community: dinoflagellates, chlorophytes and diatoms. A non-metric multidimensional scaling plot was made from the Bray–Curtis community dissimilarity distances. The envfit() function was then used to fit the best subsets of variables onto the community dissimilarity ordinations (Supporting Table 12).

Acknowledgements

We thank scientists and staff from the Galápagos Science Center (GSC), Universidad San Francisco de Quito (USFQ) and Galápagos National Park (GNP) for their logistical support during the cruises. We are grateful to Steve Walsh (UNC), Carlos Mena (USFQ) and Phil Page (UNC) for their efforts in coordinating the Galápagos Marine Expeditions. Others include Juan Pablo Muñoz (GSC), Leandro Vaca (GSC), Eduardo Espinoza (GNP), Jennifer Suarez (GNP) and the crew of the M/V Sierra Negra. We thank Sara Haines for her assistance with processing and visualizing physical and chemical observations. We are grateful to Kimberly DeLong, Sharla Sugierski and Wilton Burns for assistance with sample analyses. Natalie Cohen, Robert Lampe, and Se Hyeon Jang provided helpful comments on the manuscript. Funding for this project was provided to A.M.,

H.S. and S.G from the Center for Galápagos Studies (Office of the Vice Chancellor for Research) and the UNC College of Arts and Sciences, to E.N. by the Andrew Marion Blackmon family trust and a National Science Foundation grant to A.M. (OCE1751805).

References

Anderson, D.M., Coats, D.W., and Tyler, M.A. (1985) Encystment of the dinoflagellate *Gyrodinium uncatenum*: temperature and nutrient effects. *J Phycol* **21**: 200–206.

Barber, R.T., and Chavez, F.P. (1991) Regulation of primary productivity rate in the equatorial Pacific. *Limnol Oceanogr* **36**: 1803–1808.

Barber, R.T., Sanderson, M.P., Lindley, S.T., Chai, F., Newton, J., Trees, C.C., *et al*. (1996) Primary productivity and its regulation in the equatorial Pacific during and following the 1991–1992 El Niño. *Deep-Sea Res II Top Stud Oceanogr* **43**: 933–969.

Behrenfeld, M.J., Bale, A.J., Kolber, Z.S., Aiken, J., and Falkowski, P.G. (1996) Confirmation of iron limitation of phytoplankton photosynthesis in the equatorial Pacific Ocean. *Nature* **383**: 508–511.

Bensted-Smith, R. (1998) The special law for Galápagos. *Noticias de Galápagos* **59**.6.

Bravo, I., and Figueroa, R. (2014) Towards an ecological understanding of dinoflagellate cyst functions. *Microorganisms* **2**: 11–32.

Carnicer, O., De La Fuente, P., Canepa, A., Keith, I., Rebolledo-Monsalve, E., Diogène, J., and Fernández-Tejedor, M. (2019) Marine dinoflagellate assemblage in the Galápagos marine reserve. *Front Mar Sci* **6**: 235.

Chavez, F.P., and Brusca, R.C. (1991) The Galápagos Islands and their relation to oceanographic processes in the tropical Pacific. In *Galapagos Marine Invertebrates*. Boston, MA: Springer, pp. 9–33.

Chavez, F.P., Buck, K.R., Service, S.K., Newton, J., and Barber, R.T. (1996) Phytoplankton variability in the central and eastern tropical pacific. *Deep-Sea Res Part II: Top Stud Oceanogr* **43**: 835–870.

Clarke, K.R., and Ainsworth, M. (1993) A method of linking multivariate community structure to environmental variables. *Mar Ecol Prog Ser* **92**: 205–219.

Clarke, L.J., Bestley, S., Bissett, A., and Deagle, B.E. (2019) A globally distributed Syndiniales parasite dominates the Southern Ocean micro-eukaryote community near the sea-ice edge. *ISME J* **13**: 734–737.

Collado-Fabbri, S., Vaulot, D., and Ulloa, O. (2011) Structure and seasonal dynamics of the eukaryotic picophytoplankton community in a wind-driven coastal upwelling ecosystem. *Limnol Oceanogr* **56**: 2334–2346.

De Vargas, C., Audic, S., Henry, N., Decelle, J., Mahé, F., Logares, R., *et al*. (2015) Eukaryotic plankton diversity in the sunlit ocean. *Science* **348**: 7–8.

Dugdale, R.C., and Goering, J.J. (1967) Uptake of new and regenerated forms of nitrogen in primary productivity. *Limnol Oceanogr* **12**: 196–206.

Edgar, G.J., Bustamante, R.H., Farina, J.M., Calvopina, M., Martinez, C., and Toral-Granda, M.V. (2004) Bias in evaluating the effects of marine protected areas: the importance of baseline data for the Galapagos Marine Reserve. *Environ Conserv* **31**: 212–218.

Feldman, G.C. (1986) Patterns of phytoplankton production around the Galapagos Islands. In *Tidal Mixing and Plankton Dynamics*. New York, NY: Springer, pp. 77–106.

Fiedler, P.C., and Talley, L.D. (2006) Hydrography of the eastern tropical Pacific: a review. *Prog Oceanogr* **69**: 143–180.

Gifford, S.M., Zhao, L., Stemple, B., DeLong, K., Medeiros, P.M., Seim, H., and Marchetti, A. (2020) Microbial niche diversification in the Galápagos Archipelago and its response to El Niño. *Front Microbiol* **11**: 2636.

Guillou, L., Viprey, M., Chambouvet, A., Welsh, R.M., Kirkham, A.R., Massana, R., *et al*. (2008) Widespread occurrence and genetic diversity of marine parasitoids belonging to Syndiniales (Alveolata). *Environ Microbiol* **10**: 3349–3365.

Hama, T., Miyazaki, T., Ogawa, Y., Iwakuma, T., Takahashi, M., Otsuki, A., and Ichimura, S. (1983) Measurement of photosynthetic production of a marine phytoplankton population using a stable 13 C isotope. *Mar Biol* **73**: 31–36.

Hoppenrath, M., Murray, S.A., Chomérat, N., and Horiguchi, T. (2014) *Marine Benthic Dinoflagellates: Unveiling Their Worldwide Biodiversity*: Stuttgart, Germany: Schweizerbart science publishers.

Jakoboski, J., Todd, R.E., Owens, W.B., Karnauskas, K.B., and Rudnick, D.L. (2020) Bifurcation and upwelling of the equatorial undercurrent west of the Galápagos archipelago. *J Phys Oceanogr* **50**: 887–905.

Jephcott, T.G., Alves-De-Souza, C., Gleason, F.H., Van Ogtrop, F.F., Sime-Ngando, T., Karpov, S.A., and Guillou, L. (2016) Ecological impacts of parasitic chytrids, syndiniales and perkinsids on populations of marine photosynthetic dinoflagellates. *Elsevier* **19**: 47–58.

Johnson, Z., Shyam, R., Romano, A., Mioni, C.E., Lance, V., Murray, J.W., and Zinser, E. (2010) The effect of iron-and light-limitation on phytoplankton communities of deep chlorophyll maxima of the western Pacific Ocean. *J Mar Res* **68**: 283–308.

Kessler, W.S. (2006) The circulation of the eastern tropical Pacific: a review. *Prog Oceanogr* **69**: 181–217.

Kislik, E., Mantilla, G., Torres, G., and Borbor-Córdova, M. (2017) Biological hotspots in the Galápagos Islands: exploring seasonal trends of ocean climate drivers to monitor algal blooms. *Int Scholarly Sci Res Innov* **11**: 824–834.

Lavrinienko, A., Jernfors, T., Koskimäki, J.J., Pirttilä, A.M., and Watts, P.C. (2021) Does intraspecific variation in rDNA copy number affect analysis of microbial communities? *Trends Microbiol* **29**: 19–27.

Lindley, S.T., and Barber, R.T. (1998) Phytoplankton response to natural and experimental iron addition. *Deep-Sea Res Part II: Top Stud Oceanogr* **45**: 1135–1150.

Liu, Y., Xie, L., Morrison, J.M., Kamykowski, D., and Sweet, W.V. (2014) Ocean circulation and water mass characteristics around the Galápagos Archipelago simulated by a multiscale nested ocean circulation model. *Int J Oceanogr* **2014**: 1–16.

Lopes Dos Santos, A., Pollina, T., Gourvil, P., Corre, E., Marie, D., Garrido, J.L., *et al*. (2017) Chloropicophyceae,

a new class of picophytoplanktonic prasinophytes. *Sci Rep* **7**: 1–20.

Marchetti, A., Varela, D.E., Lance, V.P., Lance, V.P., Palmucci, M., Giordano, M., and Virginia Armbrust, E. (2010) Iron and silicic acid effects on phytoplankton productivity, diversity, and chemical composition in the central equatorial Pacific Ocean. *Limnol Oceanogr* **55**: 11–29.

Masotti, I., Moulin, C., Alvain, S., Bopp, L., Tagliabue, A., and Antoine, D. (2011) Large-scale shifts in phytoplankton groups in the equatorial Pacific during ENSO cycles. *Biogeosciences* **8**: 539–550.

Maxwell, D.C. (1975) Marine primary productivity of the Galapagos Archipelago. PhD Dissertation. The Ohio State University.

McCulloch, A. (2011) A spatio-temporal context for the phytoplankton community patterns of the Galapagos Archipelago and the Northwest Florida Shelf. PhD Dissertation. North Carolina State University.

Moore, L.R., Post, A.F., Rocap, G., and Chisholm, S.W. (2002) Utilization of different nitrogen sources by the marine cyanobacteria Prochlorococcus and Synechococcus. *Limnol Oceanogr* **47**: 989–996.

Naranjo, C., and Tapia, M.E. (2015) Plancton en el canal bolívar de la isla isabela (caleta tagus), islas galápagos durante marzo de 2009. *Acta Oceanográfica del Pacífico* **20**: 71–90.

Palacios, D.M. (2002) Factors influencing the Island-mass effect of the Galápagos Archipelago. *Geophys Res Lett* **29**: 49–41.

Palacios, D.M. (2004) Seasonal patterns of sea-surface temperature and ocean color around the Galápagos: regional and local influences. *Deep-Sea Res Part II: Top Stud Oceanogr* **51**: 43–57.

Park, J., Dunne, J.P., and Stock, C.A. (2018) Ocean chlorophyll as a precursor of ENSO: an earth system modeling study. *Geophys Res Lett* **45**: 1939–1947.

Pauly, D., and Christensen, V. (1995) Primary production required to sustain global fisheries. *Nature* **374**: 255–257.

Pennington, J.T., Mahoney, K.L., Kuwahara, V.S., Kolber, D. D., Calienes, R., and Chavez, F.P. (2006) Primary production in the eastern tropical Pacific: a review. *Prog Oceanogr* **69**: 285–317.

Pitcher, G.C., Walker, D.R., Mitchell-Innes, B.A., and Moloney, C.L. (1991) Short-term variability during an anchor station study in the southern Benguela upwelling system: phytoplankton dynamics. *Prog Oceanogr* **28**: 39–64.

Pospelova, V., and Head, M.J. (2002) Islandinium brevispinosum sp. nov. (Dinoflagellata), a new organic-walled dinoflagellate cyst from modern estuarine sediments of New England (USA). *J Phycol* **38**: 593–601.

Rafter, P.A., Sigman, D.M., and Mackey, K.R.M. (2017) Recycled iron fuels new production in the eastern equatorial Pacific Ocean. *Nat Commun* **8**: 1100.

Rii, Y.M., Duhamel, S., Bidigare, R.R., Karl, D.M., Repeta, D. J., and Church, M.J. (2016) Diversity and productivity of photosynthetic picoeukaryotes in biogeochemically distinct regions of the south East Pacific Ocean. *Limnol Oceanogr* **61**: 806–824.

Sakamoto, C.M., Millero, F.J., Yao, W., Friederich, G.E., and Chavez, F.P. (1998) Surface seawater distributions of inorganic carbon and nutrients around the Galapagos Islands: results from the PlumEx experiment using automated chemical mapping. *Deep-Sea Res Part II: Top Stud Oceanogr* **45**: 1055–1071.

Salomon, P., and Stolte, W. (2010) Predicting the population dynamics in Amoebophrya parasitoids and their dinoflagellate hosts using a mathematical model. *Mar Ecol Prog Ser* **419**: 1–10.

Santoso, A., Mcphaden, M.J., and Cai, W. (2017) The defining characteristics of ENSO extremes and the strong 2015/2016 El Niño. *Rev Geophys* **55**: 1079–1129.

Sartory, D.P., and Grobbelaar, J.U. (1984) Extraction of chlorophyll a from freshwater phytoplankton for spectrophotometric analysis. *Hydrobiologia* **114**: 177–187.

Schaeffer, B.A., Morrison, J.M., Kamykowski, D., Feldman, G.C., Xie, L., Liu, Y., *et al*. (2008) Phytoplankton biomass distribution and identification of productive habitats within the Galapagos Marine Reserve by MODIS, a surface acquisition system, and in-situ measurements. *Remote Sens Environ* **112**: 3044–3054.

Shang, L., Hu, Z., Deng, Y., Liu, Y., Zhai, X., Chai, Z., *et al*. (2019) Metagenomic sequencing identifies highly diverse assemblages of dinoflagellate cysts in sediments from ships' ballast tanks. *Microorganisms* **7**: 250.

Smayda, T.J. (2000) Ecological features of harmful algal blooms in coastal upwelling ecosystems. *Afr J Mar Sci* **22**: 219–253.

Smayda, T.J., and Trainer, V.L. (2010) Dinoflagellate blooms in upwelling systems: seeding, variability, and contrasts with diatom bloom behaviour. *Prog Oceanogr* **85**: 92–107.

Sweet, W.V., Morrison, J.M., Kamykowski, D., Schaeffer, B. A., Banks, S., and McCulloch, A. (2007) Water mass seasonal variability in the Galápagos Archipelago. *Deep Sea Res Part 1 Oceanogr Res Pap* **54**: 2023–2035.

Tapia, M., and Naranjo, C. (2012) Aspectos oceanográficos del plancton y su relación con el frente ecuatorial, durante septiembre del 2011. *Acta Oceanográfica del Pacífico* **17**: 67–91.

Tilstone, G.H., Taylor, B.H., Blondeau-Patissier, D., Powell, T., Groom, S.B., Rees, A.P., and Lucas, M.I. (2015) Comparison of new and primary production models using SeaWiFS data in contrasting hydrographic zones of the northern North Atlantic. *Remote Sens Environ* **156**: 473–489.

Torres, G. (1998) Variabilidad anual del fitoplancton marino en áreas costeras de La Libertad y Manta (Ecuador), su inter-relación con eventos El Niño. *Acta Oceanográfica del Pacífico* **9**: 115–128.

Torres, G., and Tapia, M. (2000) Distribución del fitoplancton y su comportamiento en el afloramiento en las Islas Galápagos. *Acta Oceanográfica del Pacífico* **10**: 137–150.

Torres, G., and Tapia, M. (2002) Distribución del fitoplancton en la región costera del mar ecuatoriano, durante diciembre 2000. *Acta Oceanográfica del Pacífico* **11**: 63–72.

Torres, G., and Tapia, M.E. (1998) Distribución del primer nivel trófico (fitoplancton) en el Pacífico ecuatoriano,

período 1996-1997 (pre-El Niño). *Acta Oceanográfica del Pacífico* **9**: 79–94.

Yokouchi, K., Onuma, R., and Horiguchi, T. (2018) Ultrastructure and phylogeny of a new species of mixotrophic dinoflagellate, *Paragymnodinium stigmaticum* sp. nov. (Gymnodiniales, Dinophyceae). *Phycologia* **57**: 539–554. https://doi.org/10.2216/17-140.1.

Supporting Information

Additional Supporting Information may be found in the online version of this article at the publisher's web-site:

Appendix S1: Supporting Information.

Appendix S2: Supporting Information.